INTERNATIONAL JOURNAL OF
NUMERICAL ANALYSIS AND MODELING
Volume 14, Number 2, Pages 218–242

EFFICIENT ENERGY-STABLE DYNAMIC MODELING OF COMPOSITIONAL GRADING

JISHENG KOU AND SHUYU SUN

Abstract. Compositional grading in hydrocarbon reservoirs caused by the gravity force highly affects the design of production and development strategies. In this paper, we propose a novel mathematical modeling for compositional grading based on the laws of thermodynamics. Different from the traditional modeling, the proposed model can dynamically describe the evolutionary process of compositional grading, and it satisfies the energy dissipation property, which is a key feature that real systems obey. The model is formulated for the two scales of free spaces without solids (laboratory scale) and porous media (geophysical scale). For the numerical simulation, we propose a physically convex-concave splitting of the Helmholtz energy density, which leads to an energy-stable numerical method for compositional grading. Using the proposed methods, we simulate binary and tenary mixtures in the free spaces and porous media, and demonstrate that compared with the laboratory scale, the simulation at large geophysical scales has more advantages in simulating the features of compositional grading.

Key words. Compositional grading, dynamic modeling, energy stability, Peng-Robinson equation of state.

1. Introduction

In the hydrocarbon reservoirs, gravity can cause a considerable compositional variation with depth. This phenomenon is known as compositional grading [6, 8, 10, 18, 20], and it has been observed in various oil and gas-condensate reservoirs (see [6,17] and the references therein). Accurate modeling and simulation of composition variation have significant contributions to the correct design of production and development strategies [6, 20].

Because of its importance, the compositional grading phenomenon has been modeled and numerically simulated in the literature. Gibbs [7] proposed a model to calculate compositional variation under the force of gravity for an isothermal system. A formulation for non-isothermal compositional grading has also been proposed in [8] based on the stationary system assumption and theory of irreversible processes. In [20], a nonisothermal model was used to predict compositional variation in a petroleum fluid column. In [17], a continuous thermodynamic framework was presented to calculate compositional grading in hydrocarbon reservoirs, and the effect of the gravity field on the segregation characteristics of heavy fractions in the oil was established analytically using the method of moments.

The existing modeling and simulation so far can well predict the features of compositional grading at the steady states. As the PVT (pressure, volume, and temperature) conditions of a hydrocarbon reservoir are changed by the surrounding environment, the hydrocarbon mixtures shall immigrate and mix towards a new steady state. There may exist incomplete hydrocarbon mixing since complete mixing may take a long time. So in this case, a dynamic modeling is necessary since it can provide the information about the states during evolution. Moreover, the dynamic modeling is also a useful instrument to obtain the solutions at the steady

Received by the editors on July 27, 2016, and accepted on January 18, 2017.
2000 *Mathematics Subject Classification.* 65N12; 76T10; 49S05.

state. In this paper, we treat the total (free) energy as a summation of the fluid Helmholtz energy and gravitational potential energy, and based on the first law of thermodynamics, we derive an entropy equation, which yields the requirement of total energy dissipation by the second law of thermodynamics. Furthermore, combining the diffusion equations for multiple components, we derive a dynamic model for compositional grading. The proposed model satisfies the energy dissipation property, which means that a thermodynamics-consistent steady state can be achieved after a time evolution period.

Physical experiments are often applied to study the features of compositional grading. For the laboratory scale, a free space without solids is often used, and the space size may not be large due to restricted space. The proposed model is first derived for the free space, and then it is extended to the scale of porous media. Different from the free space, a porous medium usually has multi-scale structures including various porosity and geometric tortuosity, which have significant effects on this mixing process of hydrocarbon mixtures. These multi-scale physical properties are also considered in the proposed model, and as a result, the simulated results can reflect the effects of multi-scale structures.

An analytical solution is obtained for the ideal gas equation of state that describes the PVT relation by a simple linear equation. By this analytical solution, we clearly show that heavy components are concentrated toward the bottom while light components are concentrated toward the top. For realistic hydrocarbon fluids, the numerical simulation is required in practical applications since the realistic equation of state (e.g. Peng-Robinson equation of state (PR-EOS) [21]) is strongly nonlinear, and the solutions are also essentially different from the ideal gas. Phase transition also increases the complexity of compositional grading; in fact, the mixture may be split into gas and liquid phases due to gravity effect. Numerical modeling and simulation of multi-phase fluid flow at the Darcy scale and at the pore scale have been active and challenging research topics [1, 4, 5, 26–28]; this is especially true for multi-phase flow based on a realistic equation of state, which is a very challenging but also attractive research subject in recent years [11,12,15,19,23]. To simulate such problems efficiently, a stable numerical method is demanded to satisfy the energy-dissipation principle. Here, we construct a convex-concave splitting form for the Helmholtz free energy density, which leads to an efficient, energy-stable numerical method. Finally, we simulate the compositional grading of binary and tenary mixtures at a laboratory scale and a porous medium scale, and we conclude with some analysis and comments on the simulation results.

2. Energy formulations for compositional grading

We assume that hydrocarbon mixtures in a closed reservoir have fixed total moles and constant temperature. The conditions of the fixed volume, moles and temperature have been applied in the literature [9, 14, 16, 22] for instance. For a mixture composed of N components, we denote by n_i the molar density of component i, and let $\mathbf{n} = (n_1, n_2, \cdots, n_N)^T$ and $n = \sum_{i=1}^{N} n_i$. For compositional grading in the free spaces, the total (free) energy is a summation of two contributions: the Helmholtz free energy F_b, and the gravitational potential energy F_g as

$$F(\mathbf{n}) = F_b(\mathbf{n}) + F_g(\mathbf{n}), \tag{1}$$

where

$$F_b(\mathbf{n}) = \int_\Omega f_b(\mathbf{n}) d\mathbf{x}, \;\; F_g(\mathbf{n}) = \int_\Omega f_g(\mathbf{n}) d\mathbf{x}. \tag{2}$$

Here, Ω is the spatial domain. We now describe the forms of the Helmholtz free energy density f_b and gravitational potential energy density f_g. Denote by $M_{w,i}$ the molecular weight of component i, and then the mass density of the mixture is expressed as

$$\rho = \sum_{i=1}^{N} n_i M_{w,i}.$$

The gravitational potential energy density f_g has the form

$$f_g = \rho g h, \tag{3}$$

where g is the absolute value of the gravity acceleration and h is the height that is a straight distance from the bottom of Ω against the direction of gravity acceleration. Denote by H the maximum height of the domain Ω, and then $h \in [0, H]$. The Helmholtz free energy density $f_b(\mathbf{n})$ of a Peng-Robinson fluid is given by

$$f_b(\mathbf{n}) = f_b^{\text{ideal}}(\mathbf{n}) + f_b^{\text{repulsion}}(\mathbf{n}) + f_b^{\text{attraction}}(\mathbf{n}). \tag{4}$$

Their formulations can be found in the appendix of this paper.

The chemical potential μ_i of component i is defined by

$$\mu_i = \left(\frac{\partial f_b(\mathbf{n})}{\partial n_i} \right)_{T, n_1, \cdots, n_{i-1}, n_{i+1}, \cdots, n_N}. \tag{5}$$

The pressure is formulated by the chemical potentials and the Helmholtz energy density as

$$p = \sum_{i=1}^{N} n_i \mu_i - f_b. \tag{6}$$

From (6), using the chain rule $\nabla f_b = \sum_{i=1}^{N} \mu_i \nabla n_i$, the gradients of pressure and chemical potentials have the relation

$$\nabla p = \sum_{i=1}^{N} n_i \nabla \mu_i + \sum_{i=1}^{N} \mu_i \nabla n_i - \sum_{i=1}^{N} \mu_i \nabla n_i = \sum_{i=1}^{N} n_i \nabla \mu_i. \tag{7}$$

3. Dynamical models for compositional grading

In this section, we first derive a dynamical model for compositional grading in the free spaces using the laws of thermodynamics, and then we extend it to the scale of porous media.

3.1. Model formulations in the free spaces. We denote by U the internal energy of the mixture. The first law of thermodynamics gives

$$\frac{d(U + F_g)}{dt} = \frac{d\_Q}{dt}, \tag{8}$$

where Q stands for the heat transfer from the surrounding that occurs to keep the system temperature constant. We split the total entropy S into a summation of two contributions: one is the entropy of the system (denoted by S_{sys}), and the other is the entropy of the surrounding (denoted by S_{surr}) that is expressed as

$$dS_{\text{surr}} = -\frac{d\_Q}{T}. \tag{9}$$

The Helmholtz free energy and internal energy have the relation

$$U = F_b + T S_{\text{sys}}. \tag{10}$$

Using (8), (9) and (10), we get

$$\begin{aligned}\frac{dS}{dt} &= \frac{dS_{\text{sys}}}{dt} + \frac{dS_{\text{surr}}}{dt} \\ &= \frac{dS_{\text{sys}}}{dt} - \frac{1}{T}\frac{d\_Q}{dt} \\ &= \frac{dS_{\text{sys}}}{dt} - \frac{1}{T}\frac{d(U+F_g)}{dt} \\ &= -\frac{1}{T}\frac{d(F_b+F_g)}{dt} \\ &= -\frac{1}{T}\frac{dF}{dt}. \end{aligned} \tag{11}$$

According to the second law of thermodynamics, the total entropy S shall not decrease with time, so from (11) we have $\frac{dF}{dt} \leq 0$. This means that the total (free) energy of this system shall be dissipated until a steady state is reached, and thus the total (free) energy given by (1) should attain a minimum value at the steady state.

We now consider the evolutionary process of a mixture from a non-steady state to a steady state. In the absence of convection, the mass balance equation of component i is reduced into a diffusion equation as

$$\frac{\partial n_i}{\partial t} + \nabla \cdot \mathbf{J}_i = 0, \tag{12}$$

where $\mathbf{J}_i$ denotes the diffusion flux of component i. A natural boundary condition is given as

$$\mathbf{J}_i \cdot \boldsymbol{\nu}_{\partial\Omega} = 0, \tag{13}$$

where $\boldsymbol{\nu}_{\partial\Omega}$ denotes a normal unit outward vector to the boundary $\partial\Omega$ of the domain Ω. Using the equation (12) and the boundary condition (13), we can derive the energy change with time as

$$\begin{aligned}\frac{dF}{dt} &= \int_\Omega \left(\frac{df_b(\mathbf{n})}{dt} + \frac{df_g}{dt}\right) d\mathbf{x} \\ &= \int_\Omega \sum_{i=1}^{N} \left(\mu_i + M_{w,i}gh\right) \frac{\partial n_i}{\partial t} d\mathbf{x} \\ &= -\int_\Omega \sum_{i=1}^{N} \left(\mu_i + M_{w,i}gh\right) \left(\nabla \cdot \mathbf{J}_i\right) d\mathbf{x} \\ &= \int_\Omega \sum_{i=1}^{N} \mathbf{J}_i \cdot \nabla \left(\mu_i + M_{w,i}gh\right) d\mathbf{x}. \end{aligned} \tag{14}$$

The gradient $\nabla\left(\mu_i(\mathbf{n}) + M_{w,i}gh\right)$ might be non-zero for a non-steady state, and it is a primal driving force for the diffusion of each component. From (11) and (14), we obtain

$$\frac{dS}{dt} = -\frac{1}{T}\frac{dF}{dt} = -\int_\Omega \sum_{i=1}^{N} \mathbf{J}_i \cdot \frac{1}{T} \nabla \left(\mu_i(\mathbf{n}) + M_{w,i}gh\right) d\mathbf{x} \geq 0, \tag{15}$$

where the last inequality is a result of the second law of thermodynamics.

A formulation of $\mathbf{J}_i$ satisfying (15) is

$$\mathbf{J}_i = -\frac{Dn_i}{RT} \nabla \left(\mu_i(\mathbf{n}) + M_{w,i}gh\right)$$

$$= -\frac{Dn_i}{RT}\left(\nabla\mu_i(\mathbf{n}) - M_{w,i}\mathbf{g}\right), \tag{16}$$

where $D > 0$ is the diffusion coefficient and $\mathbf{g} = -g\nabla h$. We assume that the diffusion coefficient is the same for all components, which can be relaxed in future work. Substituting (16) into (15) yields

$$\frac{dS}{dt} = -\frac{1}{T}\frac{dF}{dt} = \int_\Omega \sum_{i=1}^{N} \frac{Dn_i}{RT^2} |\nabla\left(\mu_i(\mathbf{n}) + M_{w,i}gh\right)|^2 d\mathbf{x} \geq 0. \tag{17}$$

We observe that the entropy increases with time, while the total (free) energy decays. Substituting (16) into (12), we obtain the diffusion equation of component i as

$$\frac{\partial n_i}{\partial t} - \nabla\cdot\frac{Dn_i}{RT}\left(\nabla\mu_i(\mathbf{n}) - M_{w,i}\mathbf{g}\right) = 0. \tag{18}$$

We note that the component mass conservation is inherently satisfied by (18) associated with the boundary condition (13) since

$$\frac{\partial}{\partial t}\int_\Omega n_i d\mathbf{x} = -\int_\Omega \nabla\cdot\mathbf{J}_i d\mathbf{x} = -\int_{\partial\Omega}\mathbf{J}_i\cdot\nu d\mathbf{x} = 0. \tag{19}$$

We sum (18) from $i = 1$ to N and get the balance equation of the overall molar density

$$\frac{\partial n}{\partial t} - \nabla\cdot\frac{D}{RT}\left(\sum_{i=1}^{N} n_i\nabla\mu_i(\mathbf{n}) - \rho\mathbf{g}\right) = 0. \tag{20}$$

With the relation (7), the balance equation (20) can be rewritten as

$$\frac{\partial n}{\partial t} - \nabla\cdot\frac{D}{RT}\left(\nabla p - \rho\mathbf{g}\right) = 0. \tag{21}$$

The equation (21) indicates that the change of the overall moles is caused by an inhomogeneous mechanical field composed of the pressure and gravity force.

At the steady state, the entropy attains the maximum value, and correspondingly the total energy has a minimum, so it means that $\frac{dF}{dt} = 0$. From (17), we get

$$\nabla\mu_i(\mathbf{n}) - M_{w,i}\mathbf{g} = 0, \tag{22}$$

and furthermore, we have

$$\nabla p = \rho\mathbf{g}. \tag{23}$$

So the equations (18) and (21) are reduced into

$$\frac{\partial n_i}{\partial t} = 0,\ \frac{\partial n}{\partial t} = 0. \tag{24}$$

We note that at the steady state, the equation (22) is consistent to the formulation in [6,7] since it shows that $(\mu_i(\mathbf{n}) + M_{w,i}gh)$ is constant in the domain, and moreover, (23) shows that the pressure and gravity force shall be in the mechanical equilibrium state.

3.2. Formulations in porous media. In a porous medium, because of the presence of solid particles, the fluids exist in the void spaces only instead of the total volume. As a result, the total free energy, Helmholtz free energy and gravitational potential energy of a fluid mixture in a porous medium shall become

$$F(\mathbf{n}) = F_b(\mathbf{n}) + F_g(\mathbf{n}),\ F_b(\mathbf{n}) = \int_\Omega \phi f_b(\mathbf{n}) d\mathbf{x},\ F_g(\mathbf{n}) = \int_\Omega \phi f_g(\mathbf{n}) d\mathbf{x}. \tag{25}$$

where ϕ represents the porosity of a porous medium. Here, we assume that the porosity may be heterogeneous in space but independent of time. In the presence of solids in porous media, the diffusion equation of component i shall also reformulated as

$$\phi \frac{\partial n_i}{\partial t} + \nabla \cdot \mathbf{J}_i = 0. \tag{26}$$

We still derive the total free energy change with time

$$\begin{aligned} \frac{dF}{dt} &= \int_\Omega \phi \left(\frac{df_b(\mathbf{n})}{dt} + \frac{df_g}{dt} \right) d\mathbf{x} \\ &= \int_\Omega \sum_{i=1}^{N} \left(\mu_i + M_{w,i} g h \right) \phi \frac{\partial n_i}{\partial t} d\mathbf{x} \\ &= \int_\Omega \sum_{i=1}^{N} \mathbf{J}_i \cdot \nabla \left(\mu_i + M_{w,i} g h \right) d\mathbf{x}. \end{aligned} \tag{27}$$

The diffusion paths of components in porous media usually deviate from the straight lines. Consequently, the diffusion coefficients must be corrected by the porosity ϕ and the tortuosity τ (see [3] and the references therein). As a analogue of (16), the formulation of the ith component diffusion flux in porous media can be expressed as

$$\mathbf{J}_i = -\frac{\phi}{\tau^2} \frac{D n_i}{RT} \left(\nabla \mu_i(\mathbf{n}) - M_{w,i} \mathbf{g} \right). \tag{28}$$

Thus, the mass balance equation for component i in porous media becomes

$$\phi \frac{\partial n_i}{\partial t} - \nabla \cdot \frac{\phi D n_i}{\tau^2 RT} \left(\nabla \mu_i(\mathbf{n}) - M_{w,i} \mathbf{g} \right) = 0, \tag{29}$$

which is associated with the boundary condition $\mathbf{J}_i \cdot \boldsymbol{\nu}_{\partial\Omega} = 0$.

Using the similar analysis to the case of free space, we can derive two key physical properties, i.e. component mass conservation and total energy dissipation, from the diffusion equations given in (29). We can also conclude that (29) leads to the equations (22) and (23) at the steady state.

Physically, geometric tortuosity is defined as the ratio of the average distance traveled by the component per unit length of the medium. While a component is diffusing in the interstitial fluid, the actual path traversed by it is generally longer than that in the absence of the solid, so we have $\tau^2 \geq 1$. On the other hand, $\tau^2 = 1$ if $\phi = 1$. In the numerical tests of this paper, we apply the following theoretical relation (see [2] and the references therein)

$$\tau^2 = \frac{1}{\phi^2}. \tag{30}$$

If the porosity has a uniform distribution in space, then we can reduce (29) as

$$\frac{\partial n_i}{\partial t} - \nabla \cdot \frac{D n_i}{\tau^2 RT} \left(\nabla \mu_i(\mathbf{n}) - M_{w,i} \mathbf{g} \right) = 0. \tag{31}$$

Comparing (31) and (18), we can see that because of tortuosity effect in porous media, it may take a very longer time for the fluids in porous media to reach the steady state.

3.3. Analytical solution of compositional grading for ideal gas. We now consider the analytical solution of (22) with the ideal gas equation of state in one-dimensional vertical domain. In [6], the molar fractions are selected as primal unknown variables, and for the ideal gas, by introducing the average molar weight of the mixture in the column, an approximate analytical solution of molar fractions has been derived based on the thermodynamic relations. Here, we take the molar densities as primal unknown variables, which can avoid to employ the average molar weight of the mixture.

In one-dimensional vertical domain, using the ideal gas equation of state, we calculate the gradient of chemical potential as

$$\frac{d\mu_i}{dz} = \frac{RT}{n_i}\frac{dn_i}{dz}, \tag{32}$$

where $z \in [0, H]$ and $H > 0$. Substituting (32) into (22) yields

$$\frac{RT}{n_i}\frac{dn_i}{dz} = -M_{w,i}g, \tag{33}$$

which can be further rewritten as

$$\frac{d\ln(n_i)}{dz} = -\frac{M_{w,i}g}{RT}. \tag{34}$$

Integration of (34) yields the following analytical solution

$$n_i = n_i^0 \exp\left(-\frac{M_{w,i}gz}{RT}\right), \tag{35}$$

where n_i^0 is the molar density of component i at $z = 0$.

For a closed system, we let n_i^t be the overall moles in the free-space domain, and then using the mass conservation for component i, we obtain

$$\begin{aligned} n_i^t &= \int_0^H n_i dz = n_i^0 \int_0^H \exp\left(-\frac{M_{w,i}gz}{RT}\right) dz \\ &= \frac{n_i^0 RT}{M_{w,i}g}\left(1 - \exp\left(-\frac{M_{w,i}gH}{RT}\right)\right), \end{aligned} \tag{36}$$

which gives

$$n_i^0 = \frac{n_i^t M_{w,i}g}{RT}\frac{\exp\left(\frac{M_{w,i}gH}{RT}\right)}{\exp\left(\frac{M_{w,i}gH}{RT}\right) - 1}. \tag{37}$$

Substituting (37) into (35), we obtain the analytical solution

$$n_i = \frac{n_i^t M_{w,i}g}{RT}\frac{\exp\left(\frac{M_{w,i}g}{RT}(H - z)\right)}{\exp\left(\frac{M_{w,i}gH}{RT}\right) - 1}. \tag{38}$$

We next consider the property of molar fractions. The overall molar density is defined as

$$n = \sum_{i=1}^{N} n_i = \sum_{i=1}^{N} n_i^0 \exp\left(-\frac{M_{w,i}gz}{RT}\right). \tag{39}$$

We further define the molar fraction of component i

$$x_i = \frac{n_i}{n} = \frac{n_i^0 \exp\left(-\frac{M_{w,i}gz}{RT}\right)}{\sum_{j=1}^{N} n_j^0 \exp\left(-\frac{M_{w,j}gz}{RT}\right)}. \tag{40}$$

The ratio between molar fractions of two components i and j is

$$\frac{x_i}{x_j} = \frac{n_i^0 \exp\left(-\frac{M_{w,i}gz}{RT}\right)}{n_j^0 \exp\left(-\frac{M_{w,j}gz}{RT}\right)} = \frac{x_i^0}{x_j^0} \exp\left(\frac{(M_{w,j} - M_{w,i})\, gz}{RT}\right). \tag{41}$$

We denote $\theta = \frac{M_{w,i}}{M_{w,j}}$, and further define

$$\varphi_{ij}(\theta, z) = \frac{x_i}{x_j} = \frac{x_i^0}{x_j^0} \exp\left(\frac{(1-\theta)\, M_{w,j} gz}{RT}\right). \tag{42}$$

The partial derivatives of $\varphi_{ij}(\theta, z)$ can be calculated as

$$\frac{\partial \varphi_{ij}}{\partial \theta} = -\frac{x_i^0}{x_j^0} \frac{M_{w,j} gz}{RT} \exp\left(\frac{(1-\theta)\, M_{w,j} gz}{RT}\right), \tag{43}$$

$$\frac{\partial \varphi_{ij}}{\partial z} = \frac{x_i^0}{x_j^0} \frac{(1-\theta)\, M_{w,j} g}{RT} \exp\left(\frac{(1-\theta)\, M_{w,j} gz}{RT}\right). \tag{44}$$

In particular, without loss of generality, we assume that $x_i^0 = x_j^0$, and then from (41), (43) and (44), we can see that if $\theta > 1$, i.e. $M_{w,i} > M_{w,j}$, we have $x_i \le x_j$ and the gap between x_i and x_j will increase as the height (z) increases. As expected, this relation indicates that heavy components are concentrated toward the bottom while light components are concentrated toward the top.

4. Physically energy-stable numerical method

In this section, we first discuss a physical observation that the Helmholtz free energy density can be split into the summation of two parts: one is convex and the other is concave. As we will see, this splitting leads to an efficient, stable, and energy-dissipated semi-implicit time marching scheme.

4.1. Convex-concave splitting for the Helmholtz free energy density. We note that the ideal contribution of Helmholtz free energy density shall be convex with respect to molar densities; otherwise, the fluid may split into multiple phases physically [23]. It can be proved by a rigorous mathematical analysis that its Hessian matrix is a diagonal positive definite matrix as

$$\frac{\partial^2 f_b^{\text{ideal}}}{\partial n_i \partial n_i} = \frac{RT}{n_i}, \ \frac{\partial^2 f_b^{\text{ideal}}}{\partial n_i \partial n_j} = 0, \ i \neq j. \tag{45}$$

For the pure substance, the repulsion force results in a convex contribution to the Helmholtz free energy density [23]. However, it is not true for multi-component mixtures ($N \ge 2$). In fact, the second derivatives of $f_b^{\text{repulsion}}$ can be calculated as

$$\frac{\partial^2 f_b^{\text{repulsion}}}{\partial n_i \partial n_j} = RT \left(\frac{b_i + b_j}{1 - bn} + \frac{n b_i b_j}{(1-bn)^2}\right). \tag{46}$$

We consider two-component case, and its Hessian matrix (denoted by $H_2^{\text{repulsion}}$) has the form

$$H_2^{\text{repulsion}} = RT \begin{pmatrix} \frac{2b_1}{1-bn} + \frac{nb_1^2}{(1-bn)^2} & \frac{b_1+b_2}{1-bn} + \frac{nb_1b_2}{(1-bn)^2} \\ \frac{b_1+b_2}{1-bn} + \frac{nb_1b_2}{(1-bn)^2} & \frac{2b_2}{1-bn} + \frac{nb_2^2}{(1-bn)^2} \end{pmatrix}. \tag{47}$$

We can see that the diagonal elements of $H_2^{\text{repulsion}}$ are positive, but its determinant is non-positive as

$$|H_2^{\text{repulsion}}| = -RT\frac{(b_1 - b_2)^2}{(1-bn)^2} \leq 0. \tag{48}$$

However, we observe that the summation of ideal and repulsion terms of the Helmholtz free energy density is still convex since the corresponding determinant has a positive value as

$$RT \begin{vmatrix} \frac{1}{n_1} + \frac{2b_1}{1-bn} + \frac{nb_1^2}{(1-bn)^2} & \frac{b_1+b_2}{1-bn} + \frac{nb_1b_2}{(1-bn)^2} \\ \frac{b_1+b_2}{1-bn} + \frac{nb_1b_2}{(1-bn)^2} & \frac{1}{n_2} + \frac{2b_2}{1-bn} + \frac{nb_2^2}{(1-bn)^2} \end{vmatrix} \geq \frac{RT}{n_1 n_2} > 0. \tag{49}$$

We have also carried out a number of numerical tests for multi-component mixtures (not presented here), which also verify the fact that the summation of the Hessian matrices of the ideal and repulsion terms is always positive definite.

For the pure substance, the attraction term is proved to result in a concave contribution to the Helmholtz free energy density [23]. However, it may be not true for multi-component mixture; indeed, we have observed in numerical tests that the maximum eigenvalue of its Hessian matrix may be slightly larger than zero in some cases (not presented here). It has been shown that the ideal term is always convex, and it is also a good approximation of the behavior of many gases. So we use the additional ideal term to construct a strict convex-concave splitting for multi-component mixture. Let us introduce an energy parameter $\lambda > 0$, and then we rewrite the Helmholtz free energy density as

$$f_b(\mathbf{n}) = f_b^{\text{convex}}(\mathbf{n}) + f_b^{\text{concave}}(\mathbf{n}), \tag{50}$$

where

$$f_b^{\text{convex}}(\mathbf{n}) = (1+\lambda)\, f_b^{\text{ideal}}(\mathbf{n}) + f_b^{\text{repulsion}}(\mathbf{n}), \tag{51}$$

$$f_b^{\text{concave}}(\mathbf{n}) = f_b^{\text{attraction}}(\mathbf{n}) - \lambda f_b^{\text{ideal}}(\mathbf{n}). \tag{52}$$

Then the chemical potential can be rewritten as

$$\mu_i(\mathbf{n}) = \mu_i^{\text{convex}}(\mathbf{n}) + \mu_i^{\text{concave}}(\mathbf{n}). \tag{53}$$

If we choose a sufficiently large λ, the strict convex-concave splitting can be achieved for the Helmholtz free energy density of multi-component mixture. But in practical computations, we need not take a very large value for λ, and indeed, we just take $\lambda = 0.1$ in our numerical tests, which is enough to gain the numerical convex-concave splitting. So we just assume that there exists a suitable $\lambda > 0$ such that $f_b^{\text{convex}}(\mathbf{n})$ is convex and $f_b^{\text{concave}}(\mathbf{n})$ is concave.

4.2. Semi-discrete schemes. We have shown that the energy dissipation (a result of maximum entropy) is an essential property in the evolutionary process to the steady state. So the numerical methods of preserving this property is more preferable. The fully explicit Euler's method for time integration does not preserve the decay for either of convex and concave functions unless a time step is really tiny (as a result, the computation will be extremely time-consuming). Moreover, there is a serious stability issue for the fully implicit Euler's scheme since it preserves the decay for a convex function, but fails for a concave function. To preserve the energy dissipation, a semi-implicit scheme is suggested to improve stability and maintain reasonable large time steps.

Let the time interval $I = (0, T_f]$, where $T_f > 0$. We divide I into M uniform subintervals $I_k = (t_k, t_{k+1}]$, where $t_0 = 0$ and $t_M = T_f$, and denote $\delta t = t_{k+1} - t_k$. For any scalar $v(t)$ or vector $\mathbf{v}(t)$, we denote by v^k or $\mathbf{v}^k$ its approximation at the time t_k. A semi-implicit, semi-discrete scheme is constructed for the dynamic equation at the free spaces (18) as

$$\frac{n_i^{k+1} - n_i^k}{\delta t} - \nabla \cdot \frac{Dn_i^k}{RT} \left(\nabla \mu_i^{\text{convex}}(\mathbf{n}^{k+1}) + \nabla \mu_i^{\text{concave}}(\mathbf{n}^k) - M_{w,i}\mathbf{g} \right) = 0. \tag{54}$$

Similarly, the semi-implicit, semi-discrete scheme is constructed for the dynamic equation in porous media (29) as

$$\frac{n_i^{k+1} - n_i^k}{\delta t} - \nabla \cdot \frac{\phi Dn_i^k}{\tau^2 RT} \left(\nabla \mu_i^{\text{convex}}(\mathbf{n}^{k+1}) + \nabla \mu_i^{\text{concave}}(\mathbf{n}^k) - M_{w,i}\mathbf{g} \right) = 0. \tag{55}$$

The boundary condition for the equations (54) and (55) is given by

$$\left(\nabla \mu_i^{\text{convex}}(\mathbf{n}^{k+1}) + \nabla \mu_i^{\text{concave}}(\mathbf{n}^k) - M_{w,i}\mathbf{g} \right) \cdot \boldsymbol{\nu}_{\partial\Omega} = 0. \tag{56}$$

Theorem 4.1. *Suppose that there exists a suitable $\lambda > 0$ such that $f_b^{\text{convex}}(\mathbf{n})$ is convex and $f_b^{\text{concave}}(\mathbf{n})$ is concave. The semi-discrete schemes defined in* (54) *and* (55) *are unconditionally energy stable; that is, for any time step $\delta t > 0$ the discrete energies satisfy*

$$F\left(\mathbf{n}^{k+1}\right) \le F\left(\mathbf{n}^k\right). \tag{57}$$

Proof. The convexity of $f_b^{\text{convex}}(\mathbf{n})$ yields

$$f_b^{\text{convex}}\left(\mathbf{n}^k\right) \ge f_b^{\text{convex}}\left(\mathbf{n}^{k+1}\right) + \sum_{i=1}^{N} \left(n_i^k - n_i^{k+1}\right) \mu_i^{\text{convex}}\left(\mathbf{n}^{k+1}\right). \tag{58}$$

The concavity of $f_b^{\text{concave}}(\mathbf{n})$ yields

$$f_b^{\text{concave}}\left(\mathbf{n}^{k+1}\right) \le f_b^{\text{concave}}\left(\mathbf{n}^k\right) + \sum_{i=1}^{N} \left(n_i^{k+1} - n_i^k\right) \mu_i^{\text{concave}}\left(\mathbf{n}^k\right). \tag{59}$$

From (58) and (59), we get

$$f_b\left(\mathbf{n}^{k+1}\right) - f_b\left(\mathbf{n}^k\right) \le \sum_{i=1}^{N} \left(n_i^{k+1} - n_i^k\right) \left(\mu_i^{\text{convex}}(\mathbf{n}^{k+1}) + \mu_i^{\text{concave}}(\mathbf{n}^k)\right). \tag{60}$$

The gravitational potential energy difference between steps k and $k+1$ has the form

$$f_g\left(\mathbf{n}^{k+1}\right) - f_g\left(\mathbf{n}^k\right) = \left(\rho^{k+1} - \rho^k\right) gh = \sum_{i=1}^{N} \left(n_i^{k+1} - n_i^k\right) M_{w,i} gh. \tag{61}$$

Denote

$$\mu_i^{\text{sim}}(\mathbf{n}^k, \mathbf{n}^{k+1}) = \mu_i^{\text{convex}}(\mathbf{n}^{k+1}) + \mu_i^{\text{concave}}(\mathbf{n}^k).$$

Multiplying both sides of (54) by $\left(\mu_i^{\text{sim}}(\mathbf{n}^k, \mathbf{n}^{k+1}) + M_{w,i}gh\right)$, and then summing it from $i = 1$ to N and integrating it over Ω, we obtain

$$\begin{aligned} &F_b\left(\mathbf{n}^{k+1}\right) - F_b\left(\mathbf{n}^k\right) + F_g\left(\mathbf{n}^{k+1}\right) - F_g\left(\mathbf{n}^k\right) \\ &\leq -\delta t \sum_{i=1}^{N} \int_\Omega \frac{Dn_i^k}{RT} \left|\nabla \mu_i^{\text{sim}}(\mathbf{n}^k, \mathbf{n}^{k+1}) - M_{w,i}\mathbf{g}\right|^2 d\mathbf{x}, \end{aligned} \tag{62}$$

where we have used the inequality (60) and the equation (61). Thus, (57) is obtained from (62). A similar proof can be carried out for the scheme (55). □

4.3. Fully discrete schemes. In this work, the Raviart-Thomas mixed finite element method [24, 25] is applied for spatial discretization. This method has been used frequently in reservoir engineering due to its local mass conservation for approximate solutions, which is a property we desire here. It has been successfully applied for solving the PR-EOS-based models [13, 23].

Let d be the spatial dimension. We define two functional spaces as

$$W = L^2(\Omega),$$

$$V = \{\mathbf{v} \in \left(L^2(\Omega)\right)^d : \ \nabla \cdot \mathbf{v} \in L^2(\Omega), \ \mathbf{v} \cdot \boldsymbol{\nu}_{\partial\Omega} = 0\}.$$

We use $(\cdot, \cdot)$ to represent the $L^2(\Omega)$ or $\left(L^2(\Omega)\right)^d$ inner product. We first rewrite (18) in a mixed weak formulation: to seek for solutions $n_i \in W$ and $\boldsymbol{J}_i \in V$ such that the following equations hold

$$\left(\frac{\partial n_i}{\partial t}, w\right) + (\nabla \cdot \boldsymbol{J}_i, w) = 0, \ w \in W, \tag{63}$$

$$\left(\frac{RT}{Dn_i}\boldsymbol{J}_i, \mathbf{v}\right) = (\mu_i(\mathbf{n}) + M_{w,i}gh, \nabla \cdot \mathbf{v}), \ \mathbf{v} \in V, \tag{64}$$

where $1 \leq i \leq N$. We assume that $\phi \in L^\infty(\Omega)$. The mixed weak formulation (29) is to seek for solutions $n_i \in W$ and $\boldsymbol{J}_i \in V$ such that the following equations hold

$$\left(\phi\frac{\partial n_i}{\partial t}, w\right) + (\nabla \cdot \boldsymbol{J}_i, w) = 0, \ w \in W, \tag{65}$$

$$\left(\frac{\tau^2 RT}{\phi Dn_i}\boldsymbol{J}_i, \mathbf{v}\right) = (\mu_i(\mathbf{n}) + M_{w,i}gh, \nabla \cdot \mathbf{v}), \ \mathbf{v} \in V, \tag{66}$$

where $1 \leq i \leq N$.

We use a quasi-uniform regular mesh $\mathcal{E}_h$ of the domain Ω. Let the approximate subspace duality $\mathbf{V}_h \subset V$ and $W_h \subset W$ be the r-th order ($r \geq 0$) Raviart-Thomas space (RT_r) of the partition $\mathcal{E}_h$. A semi-implicit, fully-discrete scheme for the dynamic equation in the free spaces is stated as: to seek for $n_{h,i}^{k+1} \in W_h$ and $\boldsymbol{J}_{h,i}^{k+1} \in V_h$ such that the following equations hold

$$\left(\frac{n_{h,i}^{k+1} - n_{h,i}^k}{\delta t}, w\right) + \left(\nabla \cdot \boldsymbol{J}_{h,i}^{k+1}, w\right) = 0, \ w \in W_h, \tag{67}$$

$$\left(\frac{RT}{Dn_{h,i}^k}\boldsymbol{J}_i^{k+1}, \mathbf{v}\right) = \left(\mu_i^{\text{convex}}(\mathbf{n}_h^{k+1}) + \mu_i^{\text{concave}}(\mathbf{n}_h^k) + M_{w,i}gh, \nabla \cdot \mathbf{v}\right), \ \mathbf{v} \in V_h, \tag{68}$$

where $1 \le i \le N$. Similarly, the semi-implicit, fully-discrete scheme for the dynamic equation in porous media is stated as: to seek for $n_{h,i}^{k+1} \in W_h$ and $\boldsymbol{J}_{h,i}^{k+1} \in V_h$ such that the following equations hold

$$\left(\phi \frac{n_{h,i}^{k+1} - n_{h,i}^{k}}{\delta t}, w\right) + \left(\nabla \cdot \boldsymbol{J}_{h,i}^{k+1}, w\right) = 0, \ w \in W_h, \tag{69}$$

$$\left(\frac{\tau^2 RT}{\phi D n_{h,i}^{k}} \boldsymbol{J}_{h,i}^{k+1}, \mathbf{v}\right) = \left(\mu_i^{\text{convex}}(\mathbf{n}_h^{k+1}) + \mu_i^{\text{concave}}(\mathbf{n}_h^{k}) + M_{w,i} g h, \nabla \cdot \mathbf{v}\right), \ \mathbf{v} \in V_h, \tag{70}$$

where $1 \le i \le N$. The above equations are associated with the discrete initial condition

$$\left(n_{h,i}^{0}, w\right) = \left(n_i^{0}, w\right), \ w \in W_h, \tag{71}$$

where n_i^0 is the initial distribution of component i in space.

Theorem 4.2. *Suppose that there exists a suitable $\lambda > 0$ such that $f_b^{\text{convex}}(\mathbf{n})$ is convex and $f_b^{\text{concave}}(\mathbf{n})$ is concave. The fully discrete schemes defined in* (67)-(68) *and* (69)-(70) *are unconditionally energy stable; that is, for any time step $\delta t > 0$, the fully discrete energies satisfy*

$$F\left(\mathbf{n}_h^{k+1}\right) \le F\left(\mathbf{n}_h^{k}\right). \tag{72}$$

Proof. Taking $w = \left(\mu_i^{\text{convex}}(\mathbf{n}_h^{k+1}) + \mu_i^{\text{concave}}(\mathbf{n}_h^{k}) + M_{w,i} g h\right)$ in (67), and then summing it from $i = 1$ to N, taking into account the inequality (60) and the equation (61), we can obtain

$$\begin{aligned} &F_b\left(\mathbf{n}_h^{k+1}\right) - F_b\left(\mathbf{n}_h^{k}\right) + F_g\left(\mathbf{n}_h^{k+1}\right) - F_g\left(\mathbf{n}_h^{k}\right) \\ &\le -\delta t \sum_{i=1}^{N} \left(\nabla \cdot \boldsymbol{J}_{h,i}^{k+1}, \mu_i^{\text{convex}}(\mathbf{n}_h^{k+1}) + \mu_i^{\text{concave}}(\mathbf{n}_h^{k}) + M_{w,i} g h\right). \end{aligned} \tag{73}$$

Taking $\mathbf{v} = \boldsymbol{J}_{h,i}^{k+1}$ in (68) yields

$$\left(\frac{RT}{D n_{h,i}^{k}} \boldsymbol{J}_{h,i}^{k+1}, \boldsymbol{J}_{h,i}^{k+1}\right) = \left(\mu_i^{\text{convex}}(\mathbf{n}_h^{k+1}) + \mu_i^{\text{concave}}(\mathbf{n}_h^{k}) + M_{w,i} g h, \nabla \cdot \boldsymbol{J}_i^{k+1}\right). \tag{74}$$

Substituting (74) into (73), we get

$$F\left(\mathbf{n}_h^{k+1}\right) - F\left(\mathbf{n}_h^{k}\right) \le -\delta t \sum_{i=1}^{N} \left(\frac{RT}{D n_{h,i}^{k}} \boldsymbol{J}_{h,i}^{k+1}, \boldsymbol{J}_{h,i}^{k+1}\right) \le 0, \tag{75}$$

which yields (72). A similar proof can be carried out for the scheme given in (69)-(70) . □

5. Numerical results

In this section, we use the proposed energy-dissipative method to simulate the component grading problems of two binary mixtures and a tenary mixture. The physical parameters for the components used in numerical tests are listed in Tables 1 and 2. In Table 1, M_w stands for the molar weight, P_c is the critical pressure, T_c is the critical temperature, and ω represents the acentric factor. In all numerical tests, the time is measured in units of the diffusion coefficient D. We take the gravitational acceleration $g = 10\text{m/s}^2$ and the ideal gas constant $R = 8.3144621\text{JK}^{-1}\text{mol}^{-1}$.

Table 1: Component physical parameters.

Component	M_w(g/mol)	P_c(bar)	T_c(K)	ω
nitrogen	28.01	33.90	126.21	0.039
methane	16.04	45.99	190.56	0.011
pentane	72.15	33.70	469.7	0.251
decane	142.28	21.1	617.7	0.489

Table 2: Binary interaction coefficients.

	methane	pentane	decane
methane	0	0.041	0.05
pentane	0.041	0	0
decane	0.05	0	0

The gravitational potential energy is taken equal to zero at the bottom point of the domain.

The energy parameter $\lambda = 0.1$ in (51) and (52) is taken for all numerical examples. Newton's method is used as the nonlinear solver for each time steps, and its stop criterion is that the 2-norm of the relative variation of molar density between the current and previous iterations or the 2-norm of residual errors of nonlinear functions is less than 10^{-7}. We also take the total number of Newton's iterations to be not larger than 30 for preventing infinite loops. We employ the lowest order Raviart-Thomas space (RT_0), and moreover, apply the trapezoid quadrature rule to decouple the system and to get explicit formula for each individual diffusive flux.

In the compositional grading problems, the vertical distribution of different components is primarily concerned, and their horizontal distribution is generally considered as homogeneous. So we consider one-dimensional vertical domain in numerical tests.

5.1. Binary mixture: methane and nitrogen. We test a binary mixture composed of methane (CH4) and nitrogen (N2) to verify the analytical solutions and the validity and effectivity of the proposed method. The binary interaction coefficient between methane and nitrogen is 0.1. We consider an one-dimensional vertical domain with the depth 500m, and use a uniform mesh with 500 elements. The domain is a closed free space without solids. The time step size is taken as $5 \times 10^3 D$, and 50 time steps are simulated. Both components have the same initial molar density $10\mathrm{mol/m}^3$, which is homogeneously distributed in space. The temperature is 320K. In this case, this binary mixture behaves closely to the ideal gas.

The strict dissipation of the total energy with time steps is clearly illustrated in Figure 1(a). Figure 1(b) is a zoom-in plot of Figures 1(a) in the later time steps, demonstrating that the total energy remains to decrease all the time. The convergence history verifies the energy decay property of the proposed method.

We illustrate the analytical and simulated molar densities and molar fractions in Figure 2. The analytical solutions are calculated by the formulations presented in Subsection 3.3, which are derived on the basis of the ideal gas equation of state. The numerical simulation uses the realistic PR-EOS, but in this tested case, PR-EOS reduces closely to the ideal gas equation of state because the molecular volume and

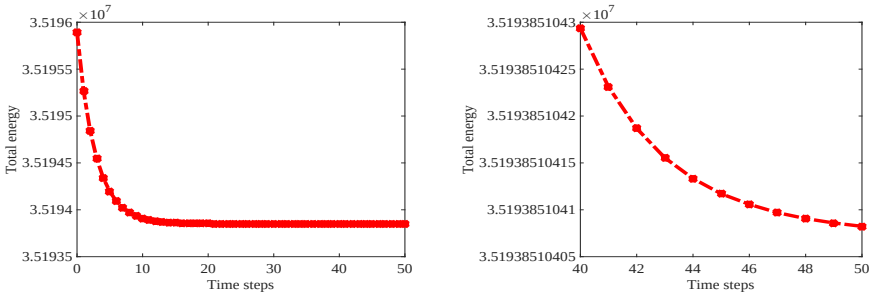

(a) (b)

Figure 1: Energy dissipation with time steps in the verification test.

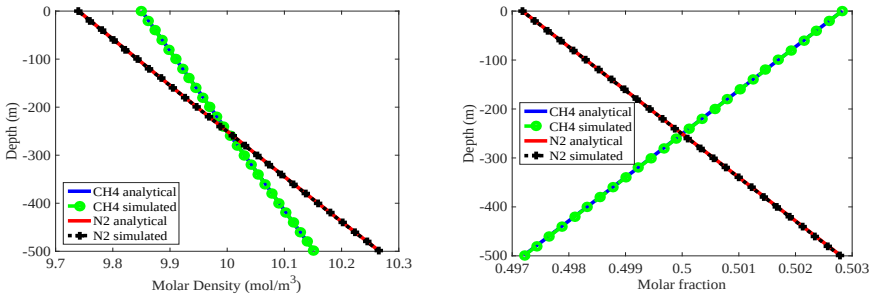

(a) (b)

Figure 2: Comparison between analytical and simulated results: molar density (a) and molar fraction (b).

interaction forces between molecules are negligible. We plot analytical and simulation results together for comparison, but the latter is highlighted with different markers. Although there exist the tiny errors caused by the models, we can observe from Figure 2 that the simulation results match the analytical solutions well. These results verify the validity of the proposed method.

We can see from Figure 2 that the gap of molar fractions between two components increases as the depth goes away from the molar fraction intersection point of two components. This verifies our conjecture drawn from the analytical solutions, which states that heavy components are concentrated toward the bottom while light components are concentrated toward the top.

5.2. Binary mixture: methane and decane. We simulate the compositional grading of a binary mixture composed of methane (CH4) and decane (nC10) at a laboratory scale and a porous medium scale. The temperature of the system keeps 381K. For the laboratory scale, a free space without solids is often used, and the space size may also not be large due to restricted space. As an example of the laboratory scale, we consider an one-dimensional vertical free space with the depth 1m, and use a uniform mesh with 100 elements. Large scale is a spatial feature of the realistic reservoir. For the problem at the porous medium scale, we need to consider an one-dimensional vertical porous medium with the depth 2000m;

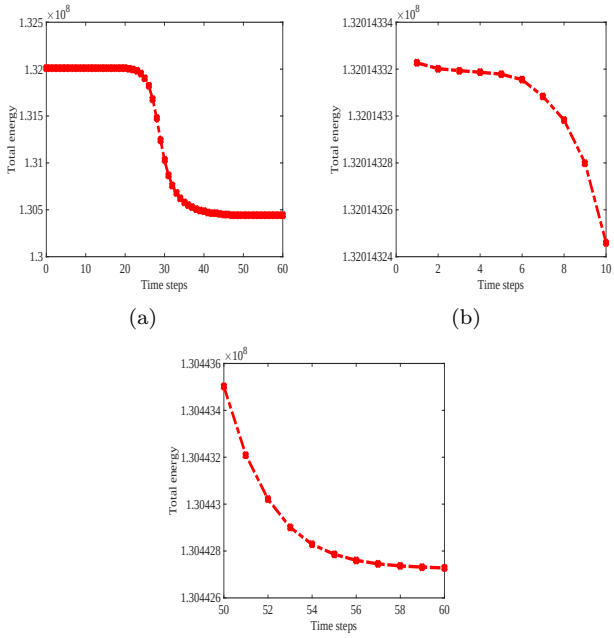

Figure 3: Binary mixture in a free space: energy dissipation with time steps.

its porosity is 0.1. A uniform mesh with 2000 elements is applied for the porous medium domain.

In the initial time, methane and decane have the uniform distributions in space with molar densities 5000 mol/m^3 and 2000 mol/m^3 respectively. For the laboratory scale problem, the time size is uniformly equal to $10^3 D$, and 60 time steps are simulated. For the problem in the porous medium, the time size is uniformly equal to $10^7 D$, and 70 time steps are simulated. In order to attain the steady state, fluids in porous media usually take a very longer time than that in the laboratory scale.

Figures 3(a) and 4(a) depict the convergence history of the proposed method, and the total energy always decays with time steps for both cases of the free space and porous medium. Figures 3(b-c) and 4(b-c) are the zoom-in plots of Figures 3(a) and 4(a) in the early and later time steps, which demonstrate that the total energy remains to decrease all the time. It is observed from Figures 3(a) that the energy decay is slow initially, and then fast in a few time steps, but quickly slows down at later time steps when the solutions approach its steady state. The phase splitting can speed up the dissipation of the total energy largely; once the phase splitting is complete, the components within each phase will rearrange their distributions due to gravity effect, but this process leads to a slow dissipation of the total energy.

In Figures 5 and 6, we illustrate the spatial variations of each component molar density and molar fraction with time steps for the free space problem. In Figures 7 and 8, we illustrate the spatial variations of each component molar density and molar fraction with time steps for the problem in a porous medium. It is observed that due to the gravitational effect, the light component (methane) is concentrated toward the top, while the heavy component (decane) is concentrated toward the

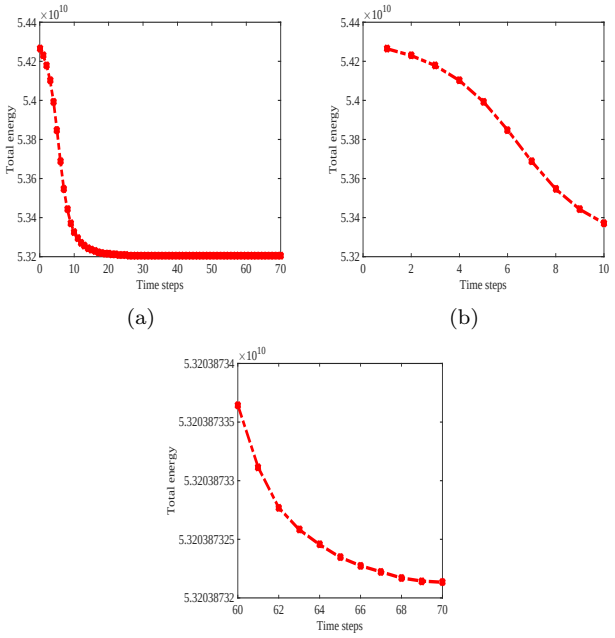

Figure 4: Binary mixture in a porous medium: energy dissipation with time steps.

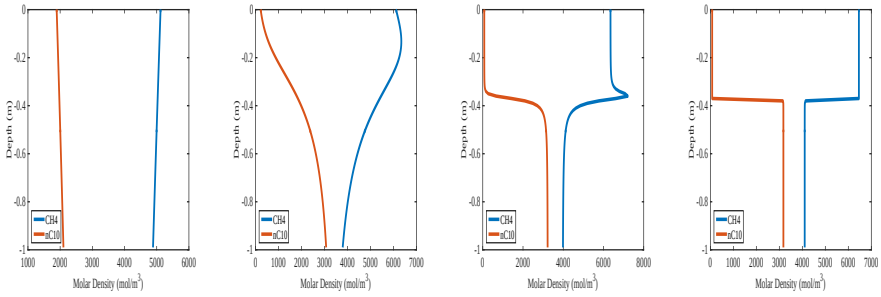

Figure 5: Binary mixture in a free space: molar densities at the 20th(a), 30th(b), 40th(c) and 60th(d) time step respectively.

bottom. We also observe that the original single-phase mixture is gradually split into the gas and liquid phases, which distribute in the different regions due to the gravitational effect, and methane tends to concentrate at the interface of two phases when the phase transition occurs. At the steady state, there is a jump in molar density between the gas and liquid regions.

Comparing the results in Figures 7 and 8 with those in Figures 5 and 6, we can see that the compositional variation in space is quite distinct in the case of porous medium, but not clear for the case of free space. This is because the gravity force is

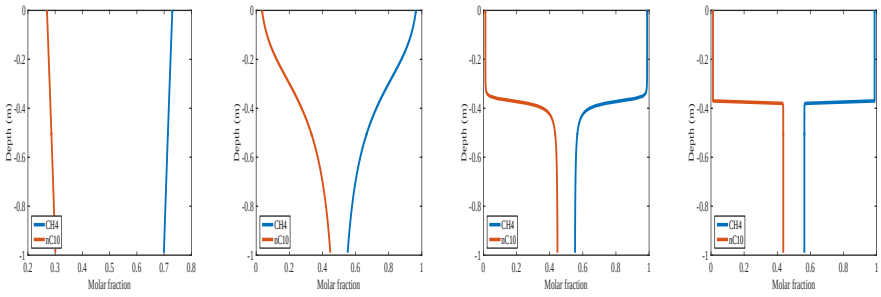

(a) (b) (c) (d)

Figure 6: Binary mixture in a free space: molar fractions at the 20th(a), 30th(b), 40th(c) and 60th(d) time step respectively.

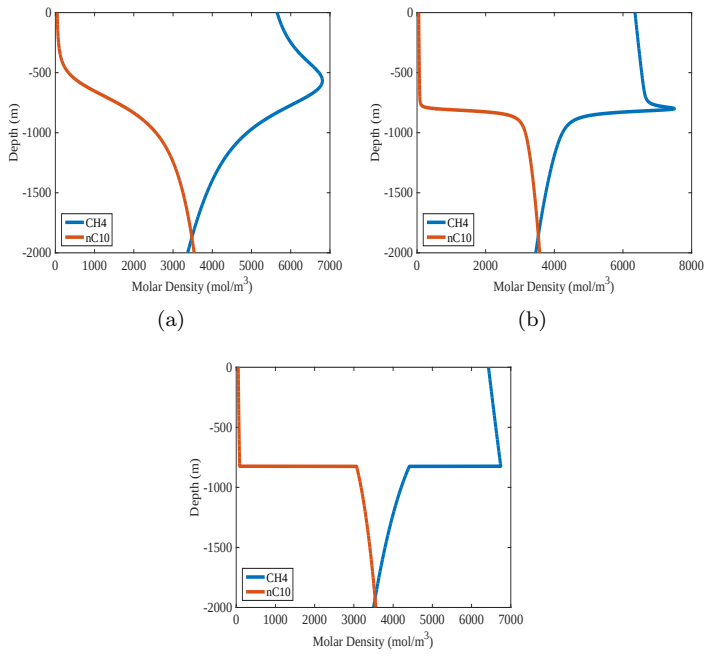

(a) (b)

(c)

Figure 7: Binary mixture in a porous medium: molar densities at the 10th(a), 20th(b), and 70th(c) time step respectively.

smaller than the chemical potential, so its effect on the compositional distribution is observed clearly only over a very long range. The results at the scale of porous media may have greater potential applications to practicing engineers than those at the laboratory scale.

5.3. Tenary mixture. The tenary mixture is composed of methane (CH4), pentane (nC5) and decane (nC10). The temperature is 370K. For the laboratory scale,

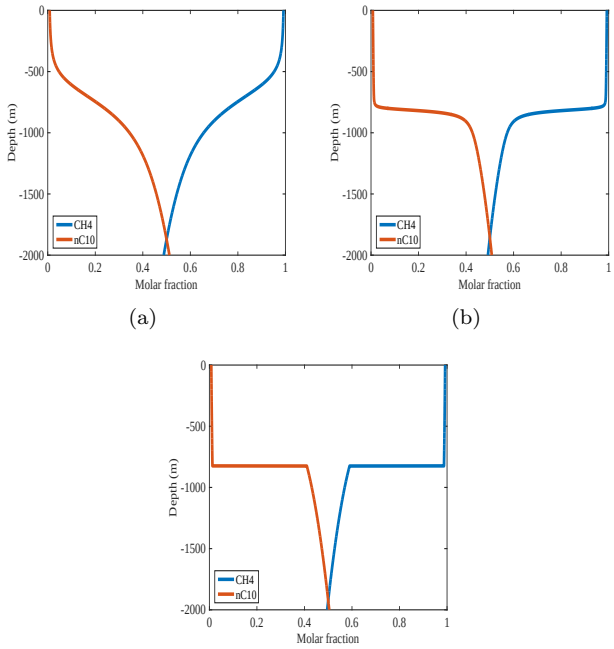

Figure 8: Binary mixture in a porous medium: molar fractions at the 10th(a), 20th(b), and 70th(c) time step respectively.

we consider an one-dimensional vertical free space with the depth 1m, and apply a uniform mesh with 100 elements. For the large scale problem in a porous medium, we consider an one-dimensional vertical porous medium with the depth 1000m. The porosity jump often occurs between different layers along the reservoir depth. In this test, a porosity jump is set in this medium; more precisely, its lower half part has the porosity 0.1, while the porosity of its upper half part is 0.5. This means that the porous medium has two-scale structure. A uniform mesh with 1000 elements is applied for the porous medium domain.

In the initial time, methane, pentane and decane have the uniform distributions in space with molar densities 3000 mol/m^3, 2000 mol/m^3 and 1000 mol/m^3 respectively. For the laboratory scale problem, the time size is uniformly equal to $5 \times 10^2 D$, and 60 time steps are simulated. For the problem in the porous medium, the time size is uniformly equal to $10^6 D$, and 80 time steps are simulated. These time setting can ensure the fluids to attain the steady states.

The total energy variation with time steps is illustrated in Figures 9(a) and 10(a) for both cases of the free space and porous medium. Figures 9(b)-(c) and 10(b)-(c) plot the energy-dissipation profiles of the early and later time steps. The strict dissipation of the total energy with time steps is also shown in these results. The effectivity of the proposed method is verified again.

In Figures 11 and 12, we illustrate the spatial variations of the overall molar density and component molar fraction with time steps for the free space problem. It is observed that the original single-phase mixture is gradually split into the gas

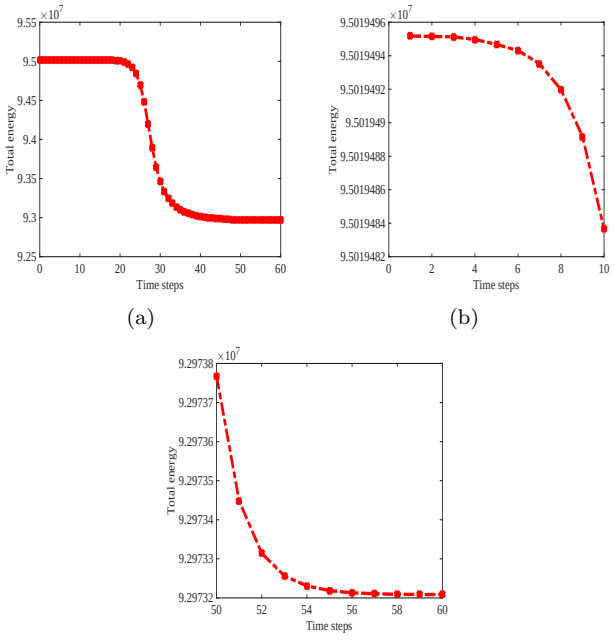

Figure 9: Tenary mixture in a free space: energy dissipation with time steps.

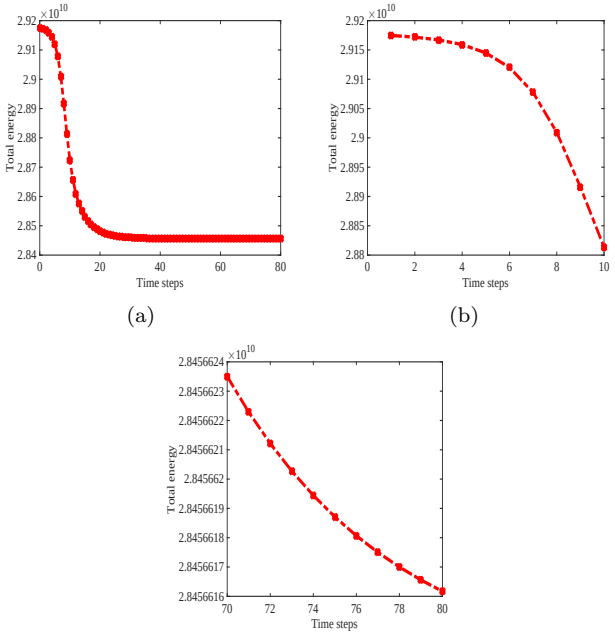

Figure 10: Tenary mixture in a porous medium: energy dissipation with time steps.

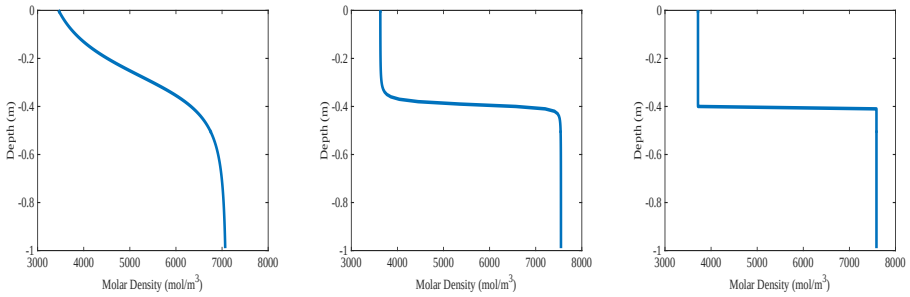

Figure 11: Tenary mixture in a free space: overall molar densities at the 30th(a), 40th(b), and 60th(c) time step respectively.

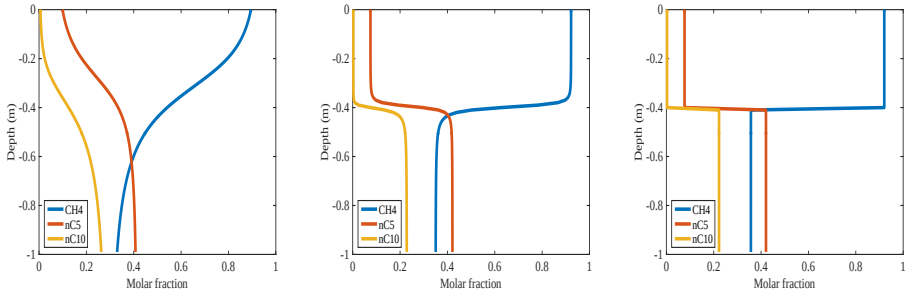

Figure 12: Tenary mixture in a free space: molar fractions at the 30th(a), 40th(b), and 60th(c) time step respectively.

and liquid phases, and moreover, due to the gravitational effect, the gas phase tends to go up toward the top, while the liquid phase is going toward the bottom.

In Figures 13 and 14, we illustrate the spatial variations of the overall molar density and component molar fraction with time steps for the problem in the porous medium. We also observe that the original single-phase mixture is gradually split into the gas and liquid phases, which tend to concentrate in the different regions due to the gravitational effect. Two-scale porosities lead to a large variation of overall molar density and molar fractions at the porosity jump.

Figures 15 and 16 depict the ratios of molar fractions between two different components at the stead state, which are the proportions of molar fraction of a light component to that of a heavy component. In particular, Figures 15(d)-(f) and 16(d)-(f) are the zoom-in plots of Figures 15(a)-(c) and 16(a)-(c), respectively. We can see that the compositional variation in space is quite distinct in the case of porous medium, but not too clear for the case of free space. It is observed from Figure 15 and 16 that due to the gravitational effect, the light component is concentrated toward the top, while the heavy component (decane) is concentrated toward the bottom. In particular, the liquid phase also behaves this trend. Moreover, this phenomenon is more discernible in quantity at the porous medium scale than at

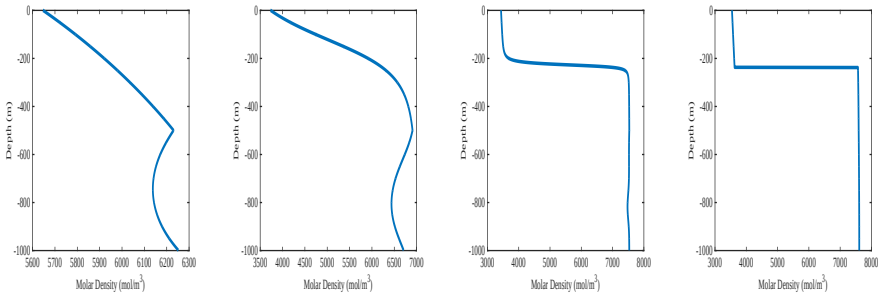

(a) (b) (c) (d)

Figure 13: Tenary mixture in a porous medium: overall molar densities at the 5th(a), 10th(b), 20th(c), and 80th(d) time step respectively.

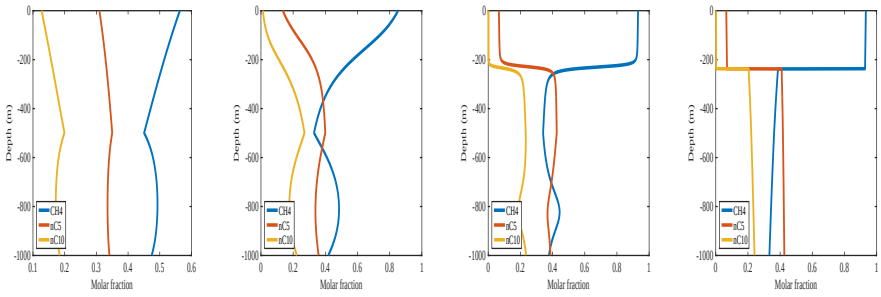

(a) (b) (c) (d)

Figure 14: Tenary mixture in a porous medium: molar fractions at the 5th(a), 10th(b), 20th(c), and 80th(d) time step respectively.

the laboratory scale. The simulation at the scale of porous media may have greater advantages than those at the laboratory scale for compositional grading.

6. Conclusions

We derive a dynamic model to simulate compositional grading in hydrocarbon reservoirs caused by the gravity force. The derivations are based on the laws of thermodynamics and multi-component diffusion equations. The formulations are applied for the two scales of free spaces and porous media. Furthermore, we propose a novel and physically convex-concave splitting of the Helmholtz energy density, which leads to an energy-stable numerical method. Finally, the proposed method is used to simulate binary and tenary mixtures in the free spaces (laboratory scale) and porous media (geophysical scale), and the validity and effectivity of the proposed method are verified. The numerical results demonstrate that compared with the laboratory scale, the simulation at large geophysical scales can clearly characterize the features of compositional grading. The effect of capillarity will be considered in the future work.

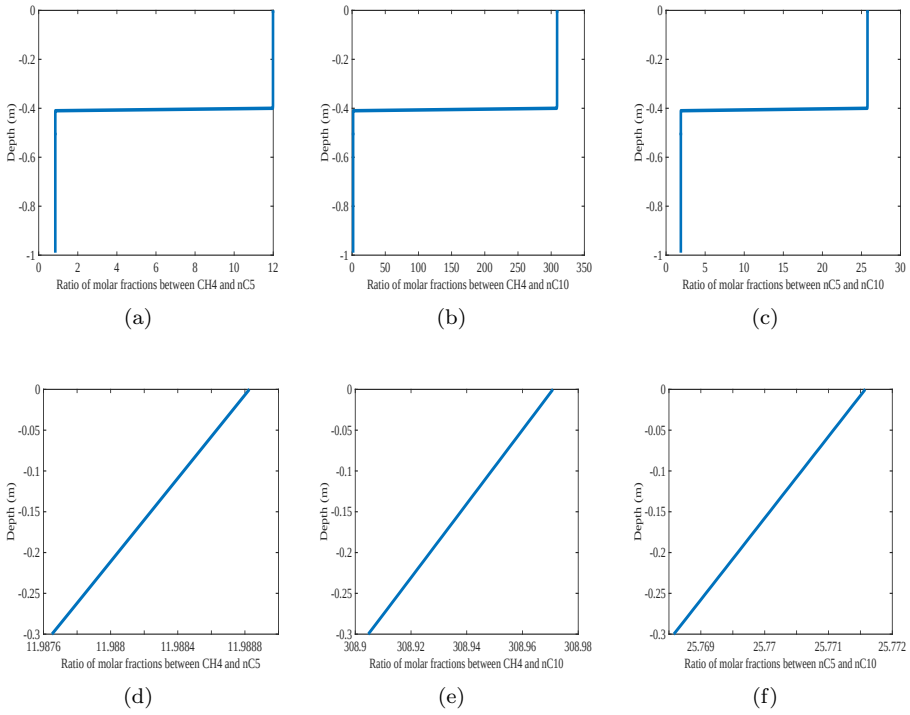

Figure 15: Tenary mixture in a free space: molar fraction ratios between two components.

Acknowledgments

This work is supported by National Natural Science Foundation of China (No. 11301163), and KAUST research fund to the Computational Transport Phenomena Laboratory.

Appendix

In the appendix, we state the formulations of the Helmholtz energy density f_b as below:

$$f_b^{\text{ideal}}(\mathbf{n}) = RT \sum_{i=1}^{N} n_i \left(\ln n_i - 1\right),$$

$$f_b^{\text{repulsion}}(\mathbf{n}) = -nRT \ln\left(1 - bn\right),$$

$$f_b^{\text{attraction}}(\mathbf{n}) = \frac{a(T)n}{2\sqrt{2}b} \ln\left(\frac{1 + (1 - \sqrt{2})bn}{1 + (1 + \sqrt{2})bn}\right),$$

where T is the thermodynamic temperature of the mixture and R is the universal gas constant. Here, b is the covolume and $a(T)$ is the energy parameter. For a mixture, these parameters are related to the ones of the pure fluids by mixing rules. Let T_{c_i}, P_{c_i} and ω_i be critical temperature, critical pressure and acentric factor, respectively, of component i. We define the reduced temperature of component i

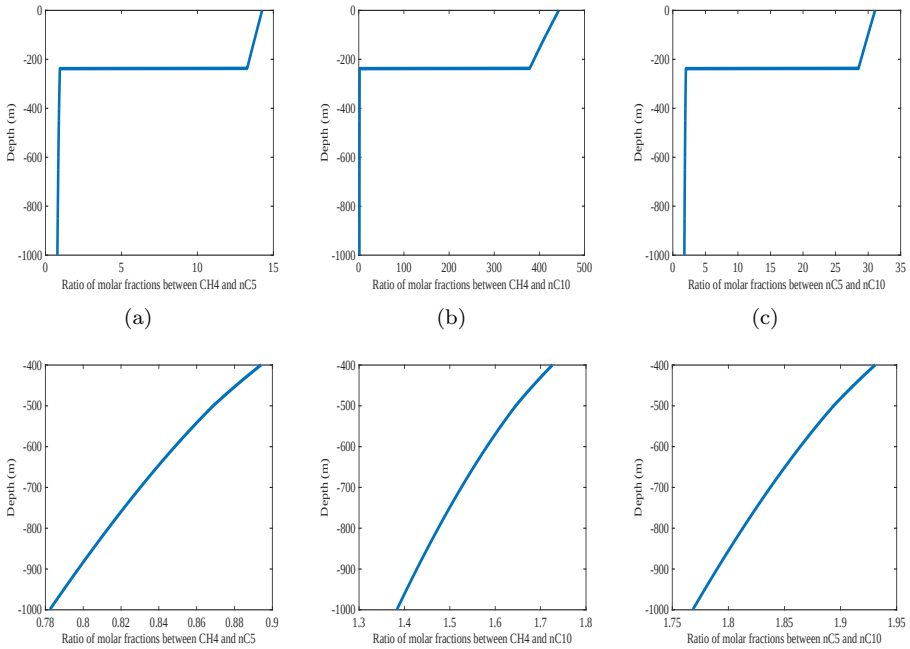

Figure 16: Tenary mixture in a porous medium: molar fraction ratios between two components.

as $T_{r_i} = T/T_{c_i}$, and furthermore, we denote the mole fraction $x_i = n_i/n$. Then we can calculate $a(T)$ and b as

$$a(T) = \sum_{i=1}^{N}\sum_{j=1}^{N} x_i x_j \left(a_i a_j\right)^{1/2}(1-k_{ij}),\ b = \sum_{i=1}^{N} x_i b_i,$$

where

$$a_i = 0.45724\frac{R^2T_{c_i}^2}{P_{c_i}}\left[1+\gamma_i(1-\sqrt{T_{r_i}})\right]^2,\ b_i = 0.07780\frac{RT_{c_i}}{P_{c_i}}.$$

Here, k_{ij} is the binary interaction coefficient between components i and j. The coefficient γ_i is computed by the acentric factor ω_i as

$$\gamma_i = 0.37464 + 1.54226\omega_i - 0.26992\omega_i^2,\ \omega_i \le 0.49,$$

$$\gamma_i = 0.379642 + 1.485030\omega_i - 0.164423\omega_i^2 + 0.016666\omega_i^3,\ \omega_i > 0.49.$$

References

[1] K. Bao and Y. Shi and S. Sun and X.P. Wang. A finite element method for the numerical solution of the coupled Cahn-Hilliard and Navier-Stokes system for moving contact line problems, Journal of Computational Physics, 231(24): 8083–8099, 2012.

[2] J. Bear and A. H.-D. Cheng. Modeling groundwater flow and contaminant transport. Springer Science & Business Media, 2010

[3] Z. Chen, G. Huan and Y. Ma. Computational methods for multiphase flows in porous media. SIAM Comp. Sci. Eng., Philadelphia, 2006.

[4] C. Dawson, S. Sun, and M.F. Wheeler. Compatible algorithms for coupled flow and transport. Computer Methods in Applied Mechanics and Engineering, 193:2565–2580, 2004.
[5] V. J. Ervin, E. W. Jenkins, and S. Sun. Coupled generalized non-linear Stokes flow with flow through a porous medium. SIAM Journal on Numerical Analysis, 47(2):929–952, 2009.
[6] A. Firoozabadi. Thermodynamics of Hydrocarbon Reservoirs. McGraw-Hill New York, 1999.
[7] J. W. Gibbs. The Scientific Papers of J.W. Gibbs. Vol. 1. New York: Dover Publications, 1961.
[8] L. Høier and C. H. Whitson. Compositional grading-theory and practice. SPE Annual Technical Conference and Exhibition. Society of Petroleum Engineers, 2000.
[9] T. Jindrová and J. Mikyška. General algorithm for multiphase equilibria calculation at given volume, temperature, and moles. Fluid Phase Equilibria, 393:7–25, 2015.
[10] M. Kiani, S. Osfouri, R. Azin, S. A. M. Dehghani. Impact of fluid characterization on compositional gradient in a volatile oil reservoir. Journal of Petroleum Exploration and Production Technology, DOI 10.1007/s13202-015-0218-2, 2015.
[11] J. Kou, S. Sun, and X. Wang. Efficient numerical methods for simulating surface tension of multi-component mixtures with the gradient theory of fluid interfaces. Computer Methods in Applied Mechanics and Engineering, 292: 92–106, 2015.
[12] J. Kou and S. Sun. Numerical methods for a multi-component two-phase interface model with geometric mean influence parameters. SIAM Journal on Scientific Computing, 37(4): B543–B569, 2015.
[13] J. Kou and S. Sun. Unconditionally stable methods for simulating multi-component two-phase interface models with Peng-Robinson equation of state and various boundary conditions. Journal of Computational and Applied Mathematics, 291(1): 158–182, 2016.
[14] J. Kou, S. Sun, and X. Wang. An energy stable evolution method for simulating two-phase equilibria of multi-component fluids at constant moles, volume and temperature. Computational Geosciences, 20: 283–295, 2016.
[15] J. Kou and S. Sun. Multi-scale diffuse interface modeling of multi-component two-phase flow with partial miscibility. Journal of Computational Physics, 318: 349–372, 2016.
[16] J. Mikyška and A. Firoozabadi. A new thermodynamic function for phase-splitting at constant temperature, moles, and volume. AIChE Journal, 57(7):1897–1904, 2011.
[17] C. Lira-Galeana, A. Firoozabadi, J. M. Prausnitz. Computation of compositional grading in hydrocarbon reservoirs. Application of continuous thermodynamics. Fluid Phase Equilibria, 102(2): 143-158, 1994.
[18] R. Mokhtari, S. Ashoori, M. Seyyedattar. Optimizing gas injection in reservoirs with compositional grading: A case study. Journal of Petroleum Science and Engineering, 120: 225-238, 2014.
[19] J. Moortgat, S. Sun, and A. Firoozabadi. Compositional modeling of three-phase flow with gravity using higher-order finite element methods. Water Resources Research, 47, W05511, 2011.
[20] M. H. Nikpoor, R. Kharrat, Z. Chen. Modeling of compositional grading and plus fraction properties changes with depth in petroleum reservoirs. Petroleum Science and Technology, 29(9): 914-923, 2011.
[21] D. Peng and D.B. Robinson. A new two-constant equation of state. Industrial and Engineering Chemistry Fundamentals, 15(1):59–64, 1976.
[22] O. Polívka and J. Mikyška. Compositional modeling in porous media using constant volume flash and flux computation without the need for phase identification. Journal of Computational Physics, 272:149–169, 2014.
[23] Z. Qiao and S. Sun. Two-phase fluid simulation using a diffuse interface model with Peng-Robinson equation of state. SIAM Journal on Scientific Computing, 36(4): B708–B728, 2014.
[24] R.A. Raviart and J. M. Thomas. Primal hybrid finite element methods for 2nd order elliptic equations. Math. Comp., 31:391–413, 1977.
[25] R.A. Raviart and J. M. Thomas. A mixed finite element method for 2nd order elliptic problems. in Mathematical Aspects of the Finite Element Method, Lecture Notes in Mathematics, 606:292–315, 1977.
[26] S. Sun and M.F. Wheeler. Discontinuous Galerkin methods for coupled flow and reactive transport problems. Applied Numerical Mathematics, 52(2–3): 273–298, 2005.
[27] S. Sun and M.F. Wheeler. L2(H1) norm a posteriori error estimation for discontinuous Galerkin approximations of reactive transport problems. Journal of Scientific Computing, 22(1), 501–530, 2005.

[28] S. Sun and M.F. Wheeler. Symmetric and nonsymmetric discontinuous Galerkin methods for reactive transport in porous media. SIAM Journal on Numerical Analysis, 43(1), 195–219, 2005.

School of Mathematics and Statistics, Hubei Engineering University, Xiaogan 432000, Hubei, China

Computational Transport Phenomena Laboratory, Division of Physical Science and Engineering, King Abdullah University of Science and Technology, Thuwal 23955-6900, Kingdom of Saudi Arabia.

E-mail: shuyu.sun@kaust.edu.sa